FC. (12)

ADA027356

THIRD QUARTER APPLIED OPTICS RESEARCH REPORT

Prepared for the
Space and Missile Systems Organization
Air Force Systems Command
Los Angeles Air Force Station, California
Under contract PO 4701-75-C-0248

Approved for public release;
distribution unlimited.

Optical Sciences Center
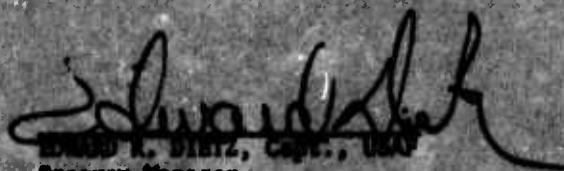University of Arizona
Tucson, Arizona 85721

1 April 1976
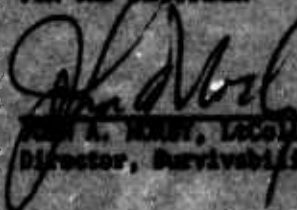
DDC

JUL 26 1976

RECEIVED

B

This report has been reviewed by the Information Office (OI) and is releasable to the National Technical Information Service (NTIS). At NTIS, it will be available to the general public, including foreign nations.

This technical report has been reviewed and is approved for publication.

EDWARD E. DIETZ, Capt., USAF
Program Manager
Survivability Directorate

FOR THE COMMANDER

JOHN A. MORBY, LtCol., USAF
Director, Survivability Directorate

REPORT DOCUMENTATION PAGE	READ INSTRUCTIONS BEFORE COMPLETING FORM

1. REPORT NUMBER	2. GOVT ACCESSION NO.	3. RECIPIENT'S CATALOG NUMBER
SAMSO TR-76-112		

4. TITLE (and Subtitle)	5. TYPE OF REPORT & PERIOD COVERED
Quarterly APPLIED OPTICS RESEARCH REPORT (Third)	Third quarter Jan. 1976–31 Mar. 1976
	6. PERFORMING ORG. REPORT NUMBER

7. AUTHOR(s)	8. CONTRACT OR GRANT NUMBER(s)
Staff of the Optical Sciences Center P. A. Franken, Director	FO 4701-75-C-0248

9. PERFORMING ORGANIZATION NAME AND ADDRESS	10. PROGRAM ELEMENT, PROJECT, TASK AREA & WORK UNIT NUMBERS
Optical Sciences Center University of Arizona 51 p. Tucson, AZ 85721	

11. CONTROLLING OFFICE NAME AND ADDRESS	12. REPORT DATE
SAMSO/DYS Los Angeles Air Force Station, California	1 April 1976
	13. NUMBER OF PAGES
	47

14. MONITORING AGENCY NAME & ADDRESS(If different from Controlling Office)	15. SECURITY CLASS. (of this report)
HQ SAMSO/DYS P.O. Box 95960, Worldway Postal Center Los Angeles, California 90009	Unclassified
	15a. DECLASSIFICATION/DOWNGRADING SCHEDULE

16. DISTRIBUTION STATEMENT (of this Report)

Approved for public release; distribution unlimited.

Rept for 1 Jan – 31 Mar 76.

17. DISTRIBUTION STATEMENT (of the abstract entered in Block 20, if different from Report)

18. SUPPLEMENTARY NOTES

19. KEY WORDS (Continue on reverse side if necessary and identify by block number)

CO_2 laser frequency
Mathematical optics
Optical wavefronts
Gratings
Lateral shear interferometer

20. ABSTRACT (Continue on reverse side if necessary and identify by block number)

This third quarter status report of the University of Arizona Optical Sciences Center presents results of work in program areas supported entirely or in part by USAF contract FO 4701-75-C-0248. Specifically covered in this report are CO_2 laser frequency, gratings, lateral shear interferometers, mathematical optics, and optical wavefronts. Also included is a list of professional publications and activities of Optical Sciences Center personnel.

DD FORM 1473 EDITION OF 1 NOV 65 IS OBSOLETE
1 JAN 73
S/N 0102-014-6601

TABLE OF CONTENTS

PROFESSIONAL PUBLICATIONS AND ACTIVITIES

OF OPTICAL SCIENCES CENTER PERSONNEL

Journal Publications (listed chronologically)

R. R. Shannon and *G. M. Sanger,* "Current status of the MMT optics,"
Opt. Eng. 14(6):544-551, November-December 1975.

L. R. Baker and R. M. Scott III, "Electro-optical remote sensors with
related optical sensors," in *Manual of Remote Sensing,* pp. 325-
366, American Society of Photogrammetry, Falls Church, Virginia,
1975.

P. N. Slater, Chap. 6, "Photographic systems for remote sensing," in
Manual of Remote Sensing, pp. 235-323, American Society of Photogram-
metry, Falls Church, Virginia, 1975.

J. G. Small, Chap. 10, "The $30 dye laser," in *The Physics of Quantum
Electronics, Vol. 4,* pp. 343-353, *S. F. Jacobs, M. Sargent III,
M. O. Scully,* and C. T. Walker, Eds., Addison-Wesley Publishing Co.,
Inc., Reading, Massachusetts, 1975.

M. O. Scully, Book Review of *Statistical Properties of Scattered Light,*
B. Crosignani, P. DiPorto, and M. Bertolotti, Eds., J. Opt. Soc. Am.
66(1):80-81, January 1976.

J. B. Hambenne and *M. Sargent III,* "Strong-signal laser operation.
I. General theory," Phys. Rev. A 13(2):784-796, February 1976.

J. B. Hambenne and *M. Sargent III,* "Strong-signal laser operation.
II. Specific cases," Phys. Rev. A 13(2):797-812, February 1976.

R. L. Shoemaker and *E. W. Van Stryland,* "Direct measurement of transition
dipole matrix elements using optical nutation," J. Chem. Phys.
64(4):1733-1740, February 1976.

C. K. Chau, *S. O. Sari* and R. E. Foster, "Pulse properties of the tunable
dye laser pulse converter," J. Appl. Phys. 47(3):1139-1141,
March 1976.

C. E. Blenman, D. L. Coffeen, T. Gehrels, C. E. KenKnight, *W. Swindell,*
and M. G. Tomasko, "The imaging photopolarimeter experiment on
Pioneer II," in *Space Research XVI,* M. J. Rycroft, Ed., Akademie-Verlag,
Berlin, 1976.

Organization of Scientific Meetings and Courses

S. Nudelman, Chairman, Session IV, "Applications of low light level devices in medicine," for the SPIE/SPSE Technical Symposium East, Reston, Virginia, 22-25 March 1976.

R. E. Wagner, Chairman, Session III, "Speckle interferometry," for the SPIE/SPSE Technical Symposium East, Reston, Virginia, 22-25 March 1976.

J. C. Wyant, General Chairman--Seminar 1, "Imaging through the atmosphere," and Chairman, Session I, "Atmospheric effects," for the SPIE/SPSE Technical Symposium East, Reston, Virginia, 22-25 March 1976.

R. R. Shannon, General Chairman for the OSA Annual Meeting, Tucson, Arizona, 18-23 October 1976.

Invited Papers

P. N. Slater, "Differences between film and solid state photographic systems," American Society of Photogrammetry Annual Meeting, Washington, D. C., 22-28 February 1976.

A. F. Turner, "Computation of the reflectance of multilayer films using vector diagrams," presented at the OSA Topical Meeting at the Asilomar Conference Center, Pacific Grove, Calif., 23-26 February 1976.

A. B. Meinel, "A modular fixed mirror Brayton cycle power system," International Conference on Solar Electricity, CNRS, Toulouse, France, 3 March 1976.

A. B. Meinel, "The exotic energy options: separating reality from illusion," Conference on Physics and Industry - International Union of Pure and Applied Physics (IUPAP), Dublin, Ireland, 10 March 1976.

M. H. Crowell, W. Nevin and S. Nudelman, "Fiber optic endoscopy with a SIT low light level television color system," presented at the SPIE/SPSE Technical Symposium East on Low Light Level Devices for Science and Technology, Reston, Virginia, 22-25 March 1976.

W. W. Metheny and R. B. Philbrick, "Separation of the optical transfer function in a turbulent medium," presented at the SPIE/SPSE Technical Symposium East on Imaging Through the Atmosphere, Reston, Virginia, 22-25 March 1976.

S. Nudelman, "Overview," presented at the SPIE/SPSE Technical Symposium East on Low Light Level Devices for Science and Technology, Reston, Virginia, 22-25 March 1976.

H. Roehrig, M. M. Frost and S. Nudelman, "High resolution low light level video systems for diagnostic radiology," presented at the SPIE/SPSE Technical Symposium East on Low Light Level Devices for Science and Technology, Reston, Virginia 22-25 March 1976.

R. R. Shannon and W. S. Smith, "An experiment for measuring effect of atmospheric turbulence on a vertical optical path," presented at the SPIE/SPSE Technical Symposium on Atmospheric Effects, Reston, Virginia, 22-25 March 1976.

R. E. Wagner, "Imagery from active optics--some pitfalls," presented at the SPIE/SPSE Technical Symposium East on Imaging Through the Atmosphere, Reston, Virginia, 22-25 March 1976.

W. L. Wolfe, E. L. Derniak and H. Roehrig, "Results on color temperature thermography," presented at the SPIE/SPSE Technical Symposium East on Low Light Level Devices for Science and Technology, Reston, Virginia, 22-25 March 1976.

Contributed Papers

B. R. Frieden, "A new restoring algorithm for the preferential enhancement of edge gradients," presented at the OSA Topical Meeting on Image Processing at the Asilomar Conference Center, Pacific Grove, California, 23-26 February 1976.

B. R. Frieden, "Maximum entropy restorations of Ganymede," presented at the OSA Topical Meeting on Image Processing at the Asilomar Conference Center, Pacific Grove, California, 23-26 February 1976.

P. N. Tamura and J. C. Wyant, "On-axis coherent optical feedback system for image processing," presented at the OSA Topical Meeting on Image Processing at the Asilomar Conference Center, Pacific Grove, California, 23-26 February 1976.

R. E. Wagner, "Post-processing of imagery from active optics," presented at the OSA Topical Meeting on Image Processing at the Asilomar Conference Center, Pacific Grove, California, 23-26 February 1976.

R. A. Schowengerdt, "A method for determining the operational imaging performance of orbital earth resources sensors," American Society of Photogrammetry Annual Meeting, Washington, D. C., 22-28 February 1976.

H. Gurev, K. D. Masterson and R. E. Hahn, "High temperature stable, spectrally selective solar absorbers for thermochemical hydrogen production," First World Hydrogen Energy Conference, Miami, Florida, March 1976.

S. O. Sari, H. Gurev and K. D. Masterson, "Interference spectroscopy in chromium-oxide-silver and silicon silver films," presented at the March meeting of American Physical Society, Atlanta, Georgia, 29 March - 1 April 1976.

Technical Reports and Government Reports

K. D. Masterson and B. O. Seraphin, "Investigation of high temperature performance of thin film, solar-thermal energy converters," Quarterly Progress Report No. 2, U.S. Bureau of Mines Gava Report, 1 October - 31 December 1975.

P. Smith, J. Coleman, A. Darling, C. Dewart, K. Macleish, A. Mclane, J. Nevins, S. Rauch, G. Schnittman, D. Smith, P. Zorn, and J. Hayes, "The design, construction, and preliminary evaluation of a solar wood heating system for a rural Vermont College," National Science Foundation, 19 December 1975.

I. Harrison, L. F. Rubin, B. Seery, and J. C. Wyant, "Optical tracking system study," Final Report, Space and Missile Test Center, Air Force System Command, Vandenberg AFB, California, January 1976.

B. O. Seraphin, "Research applied to solar-thermal power systems: chemical vapor deposition research for fabrication of solar energy converters," Final Technical Report on NSF/RANN Grant GI-36731X, January 1976.

B. O. Seraphin, "High temperature stabilization of thin metal films," Semi-Annual Progress Report, NSF/Material Sciences Division, Grant #DMR75-01267, January 1976.

R. R. Shannon and J. C. Wyant, "Optical systems evaluation," Six Month Report, Los Alamos Scientific Laboratory, University of California, Los Alamos, California, January 1976.

R. E. Hahn, H. Gurev, S. O. Sari and B. O. Seraphin, "Stabilization of thin metal films at high temperature," Semi-Annual Report, NSF Division of Material Research, Grant #DMR75-01267, 15 January 1976.

J. J. Burke, J. Geary and F. V. Richard, "Fiber optics and integrated optics in the european communist countries and Japan," Final Report for Contract DAAG 39-75-C-0137, U.S. Foreign Sciences and Technology Center, Charlottesville, Virginia, February 1976.

B. O. Seraphin, "Single layer spectrally selective coatings for high-temperature photothermal solar energy conversion," informal report on a visit to Laboratoire d'Etudes des Materiaux Minces, French Atomic Energy Commission, Grenoble, France. Submitted to NSF/Office for International Programs, February 1976.

6

S. Nudelman, T. Ovitt, Q. Fernando, D. Carter, and P. H. Bartels, "Improved instrumentation and techniques for non-invasive detection, characterization, and quantification of atherosclerosis for research and diagnostic applications," Second Quarterly Report to National Heart and Lungs Institute, 12 February 1976.

J. J. Burke, W. Wolfe, B. R. Frieden, P. H. Bartels, and J. C. Wyant, "Basic and applied research in optical science and technology," Quarterly Report for Contract F33659-72-C-0605, March 1976.

J. J. Burke, J. D. Gaskill, V. N. Mahajan, A. S. Marathay, P. Tamura, and J. C. Wyant, "Image restoration studies," Final Report, U.S. Army White Sands Missile Range, New Mexico, March 1976.

Colloquia

B. O. Seraphin, "Photothermal solar energy conversion," Exxon Corporate Research Laboratory, Linden, New Jersey, 7-9 January 1976.

H. M. Van Driel, "Hot electron photoluminescence in germanium," University of Toronto, Canada, 21 January 1976, and North Texas State University, Denton, Texas, 30 January 1976.

P. A. Franken, "Searches for chest cancers, submarines, and an ether drift," Optical Society of America as President-Elect presented at the following local chapters: Orlando, Florida, 24 January 1976; Dallas, Texas, 12 February 1976; Rochester, N.Y., 2 March 1976; Denver, Colorado, 18 March 1976; and Tucson, Arizona, 23 March 1976.

J. E. Harvey, "Surface scattering phenomena--including the inverse scattering problem," Naval Weapons Center, China Lake, California, 11 February 1976.

J. C. Wyant, "Speckle interferometry," Optical Sciences Center, Tucson, Arizona, 12 February 1976.

B. O. Seraphin, "Selective surfaces for collectors," Part I of "Solar utilization now," short course at ASU, Tempe, Arizona, 23 February 1976.

A. B. Meinel and M. P. Meinel, "Solar energy options; a review," Sheffield University, Sheffield, England, 6 March 1976.

A. B. Meinel and M. P. Meinel, "Solar energy options; a review," International Solar Energy Society - UK Section, London, England, 8 March 1976.

R. L. Shoemaker, "Time domain coherent spectroscopy," Joint Institute for Laboratory Astrophysics, University of Colorado, Boulder, Colorado, 11 March 1976.

B. O. Seraphin, "Solar energy conversion for the Winter College," at the International Centre for Theoretical Physics, Trieste, Italy, 21-26 March 1976.

8

Honors and Awards

P. A. Franken, Fellow, American Association for the Advancement of
Science.

B. R. Frieden, Fellow, Optical Society of America.

S. Nudelman, Board of Governors, S.P.I.E.

R. R. Shannon, Board of Governors, S.P.I.E.

R. L. Shoemaker, Fellow, Alfred P. Sloan Foundation.

New Committee Memberships

J. J. Burke, Member, Admissions Committee, Optical Sciences Center,
University of Arizona.

P. N. Slater, Member, Editorial Review Board, Journal of Applied
Photographic Engineering.

J. G. Small, Member, Editorial Board, The Review of Scientific
Instruments.

O. N. Stavroudis, Acting Administrator for Academic Affairs.

Public Service Speaking

K. D. Masterson, "Selective surfaces for solar thermal conversion," Course on Solar Energy, University of Arizona, Engineering Dept., NE, EE, ChE, AME 398s, February 1976.

H. Guiev, "Spectrally selective solar absorbers," IEEE Electromagnetic Compatibility Section, Tucson, Arizona, 18 February 1976.

B. O. Seraphin, "How to catch and keep a solar photon?" Optical Sciences Public Evening Lecture Series, 23 February 1976.

A. B. Meinel, "Solar energy: a new industry?" University of Arizona Extension Service, Bisbee, Arizona, 24 February 1976.

J. G. Small, "An evening of laser demonstrations," Optical Sciences Center Public Evening Lecture, 29 March 1976.

Patents and Patent Disclosures

H. H. Barrett, "Radiographic imaging system for high-energy radiation," U.S. Patent 3,936,639, 3 February 1976.

Conference Proceedings

J. C. Wyant, "Optical gauging," in *Proceedings of the SPIE Technology Utilization Program on Solving Quality Control & Reliability Problems with Optics, Vol. 60,* J. J. Amodei and H. N. Lowell, Eds., San Diego, California, 15-16 May 1976.

Y. H. Katz, A. Koso, P. N. Slater, and W. L. Wolfe, Eds., *Proceedings of the SPIE National Seminar on Scanners & Imagery Systems for Earth Observation, Vol. 51,* San Diego, California, 19-20 August 1975.

H. H. Barrett, "Fresnel zone plate and related coded apertures," in *Proceedings of the SPIE National Seminar on Coherent Optical Processing, Vol. 52,* H. J. Caulfield, Ed., San Diego, California, 21-22 August 1975.

K. Masterson, "Spectrally selective surfaces for high temperature photo-thermal solar energy conversion," in *Proceedings of the SPIE National Seminar on Optics in Solar Energy Utilization, Vol. 68,* Y. H. Katz, Ed., San Diego, California, 21-22 August 1975.

W. L. Wolfe, "Coherent and non-coherent far infrared calibration," in *Proceedings of the SPIE National Seminar on Long Wavelength Infrared, Vol. 67,* W. L. Wolfe, Ed., San Diego, California, 21-22 August 1975.

CO_2 LASER FREQUENCY AND COUPLING MODULATION USING NH_2D

(R. L. Shoemaker)

We have been continuing our research on an intracavity modulator that utilizes refractive index changes in a resonant molecular gas to provide frequency modulation of a CO_2 laser, or in a rotated configuration, to provide coupling modulation. Briefly, the device consists of a small gas cell containing NH_2D as well as a pair of metal plates separated by dielectric spacers. The cell is positioned in a CO_2 laser cavity so that the laser beam passes through the cell between the plates. The frequency of an NH_2D rotation-vibration transition can be shifted by applying an electric field across the plates. Associated with this change in absorption frequency is a relatively large change in the index of refraction and it is this index change that we are attempting to use for frequency modulation of a CO_2 laser. Further details regarding the operation of the device and its anticipated performances may be found in previous quarterly reports.

During this quarter we have finished construction of an operating version of the device and operated it successfully inside the CO_2 laser cavity. In order to do this, we had to solve a recurrence of the gas breakdown problem described in the previous quarterly report. There we noted that in tests outside the laser cavity we were able to avoid electrical breakdown of the NH_2D Stark cell by using a mixture of 2 Torr NH_2D in 10 Torr of CCl_4. However, in the experiments conducted during the past quarter, where we put the cell inside the laser cavity and looked for frequency modulation, we were initially unable to observe any effect

at all. On removing the cell from the cavity we discovered that the NH_2D absorption had entirely disappeared. Our tentative conclusion is that the action of short pulses across the cell (on top of the dc bias field of 3550 V/cm) and/or the presence of the fairly intense uv light, which is emitted from the laser discharge, is causing breakdown of the gas mixture even though no arcing can be observed.

To remedy the problem, we again began experimenting with different gas mixtures, and eventually were successful with a gas mix of 1.2 Torr of NH_2D in 14 Torr of CCl_4. When the cell containing this mixture was put inside the laser cavity, no deterioration was observed, and we had a working system. By applying a small sine wave voltage to the cell (<5 V) and looking at the variation in laser output power with a lock-in ampli-fier, we measured the linewidth of the transition to be ∿195 MH_2 FWHM. This implies a pressure broadening of NH_2D by CCl_4 of 6.6 MH_2/Torr, which is about what we had hoped for.

We were also able to verify an important and extremely desirable feature of the modulator, namely that there are no significant heating problems in the gas even though one has circulating powers of ∿60 W inside the laser cavity. This is in contrast to solid-state intracavity modu-lators such as CdTe where heating and thermal focusing problems at these power levels are substantial.

When pulses were applied to frequency modulate the laser, an unex-pected phenomenon was observed. At the beginning and end of each pulse, a spike in the laser output amplitude was observed. This amplitude spike

need not interfere with the FM modulation, but it would be interesting to understand the physics involved. We are presently investigating this phenomenon.

We have not yet been able to measure one important characteristic of the modulator, namely the frequency deviation per volt of applied electric field. This measurement requires a second stable CO_2 laser to use as a local oscillator at the detector. We have such a laser available to us, but it was not operating properly at the time when we were set up to make the test. This measurement will be made during the next quarter.

In the past week we have also received a very interesting private communication from R. L. Abrams at Hughes Aircraft Company. He has just discovered a transition in $N^{15}H_2D$ that appears to correspond with the one we are presently using in $N^{14}H_2D$. The Stark effects apparently are comparable, but in $N^{15}H_2D$ the dc bias voltage is about three times lower. Thus use of this molecule could completely eliminate the breakdown problems we have encountered with $N^{14}H_2D$ and allow the use of a more efficient gas mix. We hope to investigate this point further.

MATHEMATICAL OPTICS

(O. N. Stavroudis)

Work continues in the two principal research areas, modular optical design and the study of caustic surfaces and their application to optical design.

A paper entitled "Caustic Surfaces and the Structure of the Geometric Image" by O. N. Stavroudis and R. C. Fronczek has been submitted to the *Journal of the Optical Society of America.*

A simplified derivation of the formulas for generalized ray tracing has been obtained and a paper describing this technique is in preparation.

The study on the fifth-order aberrations associated with optical design modules, which was begun last summer, will now be completed. A paper is being prepared.

The programs for generalized ray tracing and for plotting sterescopic illustrations of wavefronts and caustics are now being revised. The new revisions should result in less expensive, more accurate plots.

A study has commenced on the practicability of using optical design modules to realize an optical layout in the form of a y-$\bar{y}$ diagram. The study will result in a dissertation proposal.

Caustic Surfaces

Some of the material in "Caustic Surfaces and the Structure of the Geometric Image" was described at some length in the previous quarterly report in which we considered the caustic associated with the rotationally

symmetric wavefront. The paper now goes far beyond this and includes the case of caustic surfaces associated with nonrotationally symmetric lenses.

The expression for the general caustic is

$$\vec{C} = -\vec{K} + \vec{S}(R + s)/2n^2$$

where $\vec{S} = (u, v, w)$ is the reduced direction cosine vector of a ray, where $\vec{K}$ is the gradient of an arbitrary function in the general solution of the eikonal equations, and where n is the refractive index. The functions R and s depend on the reduced direction cosines of a ray.

When the lens is rotationally symmetric, the vector $\vec{K}$ lies in the meridian plane. As it is a function of the reduced direction cosines of a ray, it indicates the location of the intersection of a ray with the meridian plane and therefore generates the diapoint pattern described by Herzberger.

Using these concepts it is possible to describe Herzberger's half-symmetric and symmetric images. In the half symmetric image the diapoint structure degenerates into a curve in the meridian plane. We show that this curve is exactly a degenerate sheet of the caustic surface. In the case of the symmetric image this curve becomes a straight line, which is exactly the degenerate spike-like sheet of the radially symmetric caustic. The spike is the line of symmetry of the caustic's other sheet, which is identical to the caustic produced by an axial object point in a rotationally symmetric system except that it need not coincide with the axis of the lens.

In any caustic surface a ray passing through a point where the two sheets are in contact also passes through a point in a wavefront where the two principal curvatures are equal. Such a point, called an umbilical point, is essentially spherical. The ray associated with the umbilical point is a logical choice for a chief ray because of its freedom from aberrations.

Generalized Ray Tracing

The formulas for the refraction equations in one form or another, go back at least to Coddington. Gulstrand and Kneisley as well as Stavroudis have contributed derivations, all of which suffer from an overwhelming complexity. Our new derivation is somewhat simpler although it does lean very heavily on some sophisticated mathematics.

One mechanism we use is the directional derivative. Consider a function of three variables, $f(x, y, z)$. If $\vec{V}$ is some direction vector, we can always obtain a curve $\vec{P}$ whose tangent vector is $\vec{V} = \vec{P}'$. If we take a derivative of $f(x, y, z)$ along this curve we obtain

$$\nabla f \cdot \vec{P}' = \nabla f \cdot \vec{V}.$$

Rearranging these symbols to get $(\vec{V} \cdot \nabla)f$ we obtain the same thing, but without having to refer to the space curve $\vec{P}$. This is called the derivative of f in the direction $\vec{V}$ and $(\vec{V} \cdot \nabla)$ is identified as the directional derivative operator.

The other tool is the system of Frenet equations. Using the directional derivatives these take the form

$$(\vec{t} \cdot \nabla)\vec{t} = \vec{n}/\rho, \quad (\vec{t} \cdot \nabla)\vec{n} = -\vec{t}/\rho + \vec{b}/\tau, \quad (\vec{t} \cdot \nabla)\vec{b} = -\vec{n}/\tau .$$

Here $\vec{t}$, $\vec{n}$ and $\vec{b}$ are the tangent, normal, and biaxial vectors of a space curve, respectively, and $1/\rho$ and $1/\tau$ are the curvature and torsion of that curve.

To obtain the generalized ray trace equations for refraction all we need do is take the directional derivative of Snell's law

$$\vec{N}' \times \vec{\bar{N}} = \mu(\vec{N} \times \vec{\bar{N}})$$

(a) in a direction normal to the plane of incidence and (b) in a direction in the plane of incidence tangent to the refracting surface. Applying the Frenet equations to the results of these operations yields the desired equations

$$\frac{1}{\rho_p'} = \frac{\mu}{\rho_p} + \frac{\alpha}{\bar{\rho}_p}$$

$$\frac{\cos\tau}{\tau'} = \frac{\mu\cos i}{\tau} + \frac{\alpha}{\bar{y}}$$

$$\frac{\cos^2 r}{\rho_q'} = \frac{\mu\cos^2 i}{\rho_q} + \frac{\alpha}{\bar{\rho}_q} \ .$$

Here $1/\rho_p$, $1/\rho_p'$, and $1/\bar{\rho}_p$ represent the curvatures of the incident and refracted wavefront and the refracting surface, respectively, in a direction normal to the plane of incidence. In the same sense, $1/\rho_q$, $1/\rho_q'$, and $1/\bar{\rho}_q$ represent curvatures on the same surfaces in a direction tangent to the surfaces and lying in the plane of incidence. Finally $1/\tau$, $1/\tau'$, and $1/\bar{\tau}$ represent the torsion of a geodesic curve on these surfaces in a direction normal to the incident plane.

These calculations when adjoined to the usual ray-tracing process yield a wealth of information about the aberration structure associated with a ray traced through a lens. The locus of the centers of principal curvature is exactly the caustic surface. It is these equations that are used to obtain the stereoscopic plots of caustic surfaces we have described in earlier reports.

OPTICAL WAVEFRONTS

(J. M. Geary)

We present below a study of the interaction of an optical wavefront with the aerial photographic reconnaissance window. Such interaction distorts the shape of the wavefront to a degree proportional to window quality. We discuss the optical transfer function of windows, and calculate sample MTF's.

Window Optical Transfer Function

The optical transfer function (OTF) is one method of evaluating reconnaissance windows. Strictly speaking, the OTF of a window cannot be isolated from lens considerations. We need an aperture and focusing element to be able to define upper limits on spatial resolution. The procedure will be to define a diffraction-limited imaging system whose pupil will contain phase variations attributable to the window.

The OTF or incoherent transfer function of an imaging system is defined as

$$\mathscr{H}(\nu,\eta) = \frac{1}{K} F\{|h|^2\},$$

where h is the coherent impulse response, $F\{\ \}$ is the Fourier transform, and K is a normalization factor. Taking the Fourier transform, we obtain

$$\mathscr{H}(\nu,\eta) = \frac{1}{K} H(\nu,\eta) \star\star H^*(\nu,\eta),$$

where $H(\nu,\eta)$ is the coherent transfer function. The stars indicate a two-dimensional correlation, and the asterisk designates the complex conjugate.

Now $H(\nu,\eta) = p(-\lambda f\nu, -\lambda f\eta)$, where p is the pupil function. The internal parameters contain the scaling factors $-\lambda f$, where λ is wavelength and f is the focal length. We can rewrite the OTF, then, in terms of the pupil function

$$\mathscr{H}(\nu,\eta) = \frac{1}{K} p(-\lambda f\nu, -\lambda f\eta) \star\star p^*(-\lambda f\nu, -\lambda f\eta);$$

i.e., the OTF is the normalized autocorrelation of the pupil function and $K = p(0,0) \star\star p^*(0,0)$.

Assuming a diffraction-limited lens, i.e., the angular resolution is determined by the diameter of the aperture, the unobstructed pupil function is simply $p(x,y) = \text{cyl}[\sqrt{x^2 + y^2}/d]$, where we have replaced the scaling notation, since $x = -\lambda f\nu$ and $y = -\lambda f\eta$. The quantity d is the pupil diameter.

For this situation then,

$$\mathscr{H} = \frac{1}{K} \text{cyl} \frac{\sqrt{x^2 + y^2}}{d} \star\star \text{cyl} \frac{\sqrt{x^2 + y^2}}{d} \ .$$

The asterisk is dropped because we are dealing with a real function.

When the window is inserted in front of the lens, the pupil function becomes more complicated. A phase factor must be incorporated to account for the variations in window thickness across the face of the pupil, Therefore,

$$p(x,y) \; = \; e^{ikT(x,y)} \; \mathrm{cyl} \; \frac{\sqrt{x^2 + y^2}}{d} \; ,$$

where $T(x,y)$ describes the variation in optical path and $k = 2\pi/\lambda$.
$T(x,y)$ is found in the following manner. In Fig. 8 we consider a single
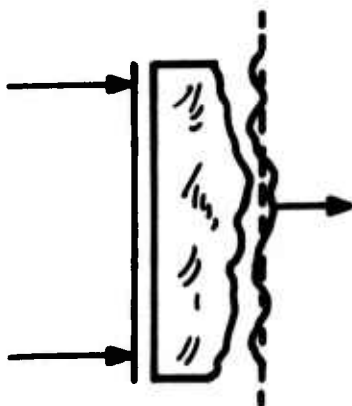pass of the incident collimated wavefront through the window.

Fig. 8. Wavefront after Single
Pass through Window.

For convenience we assume one face of the window is flat and the index
is homogeneous. The phase of the wavefront in the exit plane is found
from

$$k\{nt(x,y) + [t_0 - t(x,y)]\} \; = \; kT(x,y)$$

where $t(x,y)$ is the actual variation in thickness and t_0 is the maximum
window thickness. Setting

$$t'(x,y) \; = \; (n - 1)t(x,y),$$

we obtain

$$T(x,y) \; = \; t_0 + t'(x,y).$$

Thus

$$p(x,y) = e^{ikt_0} e^{ikt'(x,y)} \text{cyl} \frac{\sqrt{x^2 + y^2}}{d} .$$

The OTF then becomes

$$\mathcal{H} = \frac{1}{K} e^{ikt'(x,y)} \text{cyl} \frac{\sqrt{x^2 + y^2}}{d} \star\star e^{-ikt'(x,y)} \text{cyl} \frac{\sqrt{x^2 + y^2}}{d} .$$

It should be noted that fringe patterns obtained with many wave-front interferometers correspond to those for a double pass system. OTF calculations, however, correspond to a single pass system. The distinction is important. In the double pass system $\Delta t = \lambda/2n$. In OTF calculations we use $t' = (n-1)t$. Therefore, $\Delta t' = (n-1) t$. If as before we set $n = 1.5$, then $\Delta t' = (1.5-1)\lambda/3 = \lambda/6$. The thickness variation $t(x,y)$ can be determined directly from the wavefront interferometer interferogram. A functional formalization is rare; numerical analysis and the use of a computer are usually required. However, a bull's-eye pattern can be formulated easily, using

$$t'(x,y) = \frac{\lambda n}{2} N(x,y),$$

where N is the fringe-counting factor. $N = 0$ at the bull's-eye center. Also,

$$N(x,y) = \sqrt{x^2 + y^2}/\overline{\Lambda},$$

where $\overline{\Lambda}$ is the average fringe spacing. It should be noted that a bull's-eye pattern in the interferogram indicates defocus. An adjustment

bull's-eye pattern in the interferogram indicates defocus. An adjustment of focus for the pattern should improve the image quality significantly.

In most cases the OTF will be a complex quantity, i.e.,

$$OTF = \omega + i\nu.$$

Consequently the modulation transfer function (MTF) and phase transfer function (PTF) are found from

$$MTF = \sqrt{\omega^2 + \nu^2}$$

$$PTF = \tan^{-1} \frac{\nu}{\omega}.$$

In the absence of a computer, or suitable program, the MTF of a window can be calculated, albeit tediously, by hand. The procedure is now described.

Figure 9 is an enlarged drawing on which is superimposed a pure wedge grid whose spacing is the average spacing, S, between fringes in the interferogram. Pure wedge causes no image degradation. It is departure from pure wedge that does this. To obtain a sampling of pure wedge departure, three horizontal lines are drawn through the interferogram, and the intersection of these lines with interference fringes is determined. This is illustrated in Fig. 9. Each straight line in the wedge grid corresponds to one of the fringes. The positive or negative separation, s, measured along the horizontal, between the grid line and its corresponding fringe is determined for *each* sample
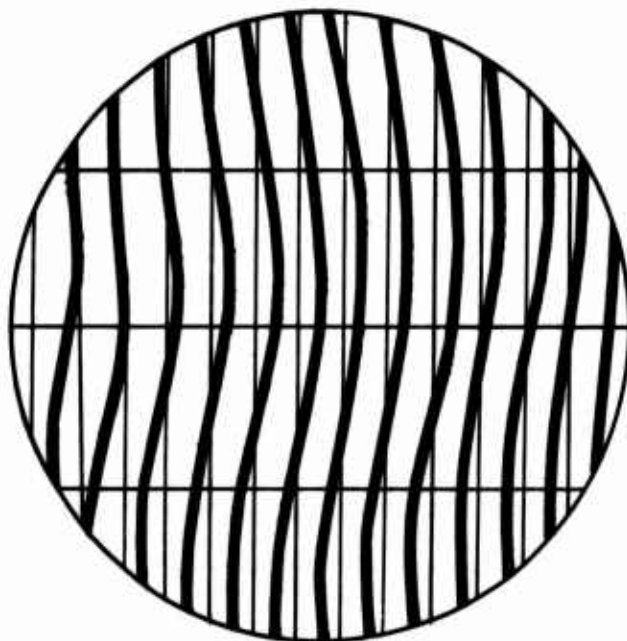
Fig. 9.   Enlarged Drawing of Interferogram with Superimposed Wedge Grid
and Horizontal Sampling Lines.

position. Once these distances are found, they must be converted into phase departures. The fringes are $\lambda/6$ or $\pi/3$ radians apart. The phase departure, ϕ, is found from

$$3S/\pi \ = \ s/\phi.$$

In the case of Fig. 9, with S equal to 0.44 in., ϕ is equal to $2.38s$.

Recall that the OTF is an autocorrelation of the pupil function; i.e., for a given shift, x, between the pupils, as illustrated in Fig. 10, there is a point-by-point multiplication of the pupils in the area of overlap. This new function is then integrated over the overlap area. This yields a single value to be assigned to the particular shift x. The shift can take on any value between 0 and d, the diameter of the pupil, and at *each* shift position the above-mentioned multiplications and integrations are made.

In practice, even on large computers, the autocorrelation is a sampled function; i.e., the autocorrelation is carried out only at discrete points. Thirty-six sample points across the pupil have been picked in our approximation.

Since there are only phase variations across the pupil under consideration, the point-by-point multiplication will turn out to be a point-by-point subtraction of the exponents. We must keep in mind that the shifted function is a complex conjugate.

In Fig. 11, the correlation procedure is illustrated. The ϕ values for each horizontal line are written out twice in two separate rows, the lower row of a set being shifted. In the illustration, the
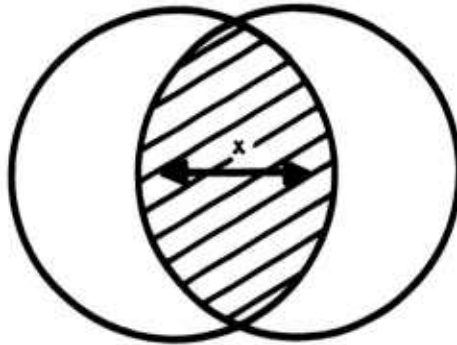
Fig. 10.   Pupil Correlation.

1:      $(\phi_{1,1} \quad \phi_{1,2} \quad \phi_{1,3} \quad \cdots \quad \phi_{1,m})$
         $-(\phi_{1,1} \quad \phi_{1,2} \qquad \cdots \quad \phi_{1,m})$

2:      $(\phi_{2,1} \quad \phi_{2,2} \quad \phi_{2,3} \quad \cdots \quad \phi_{2,m})$
         $-(\phi_{2,1} \quad \phi_{2,2} \qquad \cdots \quad \phi_{2,m})$

3:      $(\phi_{3,1} \quad \phi_{3,2} \quad \phi_{3,3} \quad \cdots \quad \phi_{3,m})$
         $-(\phi_{3,2} \quad \phi_{3,2} \qquad \cdots \quad \phi_{3,m})$

Fig. 11.   Illustration of Correlation.

shift is one unit. A shift unit corresponds to the average spacing, S.

We obtain the sum

$$\sum_{\substack{j=1 \to 3 \\ k=(1+shift) \to m \\ l=k-shift}} e^{i[\phi_{jk}-\phi_{jl}]} = \sum (\cos\phi + i\sin\phi)$$

where

$$\phi = [\phi_{jk} - \phi_{jl}].$$

We then calculate all the $\cos\phi$'s and sum, and all the $\sin\phi$'s and sum. This yields a complex number $U(NS) + iV(NS)$, where N is an integer, which is a function of the shift position. This becomes the OTF after normalization by the number of sample points (36 in this case). The MTF is found from $(U^2 + V^2)^{\frac{1}{2}}/36$.

The MTF's corresponding to two windows as well as the theoretical MTF for a 24-in. $f/6.6$ lens are presented in Fig. 12. The cutoff frequency is found from the relationship stated earlier, $x = \lambda f\nu$, when $x = d$. Therefore, $\nu_c = d/\lambda f = 300$ 1/mm for $d = 3.6$ in., $f = 24$ in., $\lambda = 500$ μm.

Better MTF approximations can be obtained by increasing the number of samples.

Criterion for Selecting Windows

We have looked at the OTF as a means of evaluating window quality and have seen that for the most part it is a complicated and time
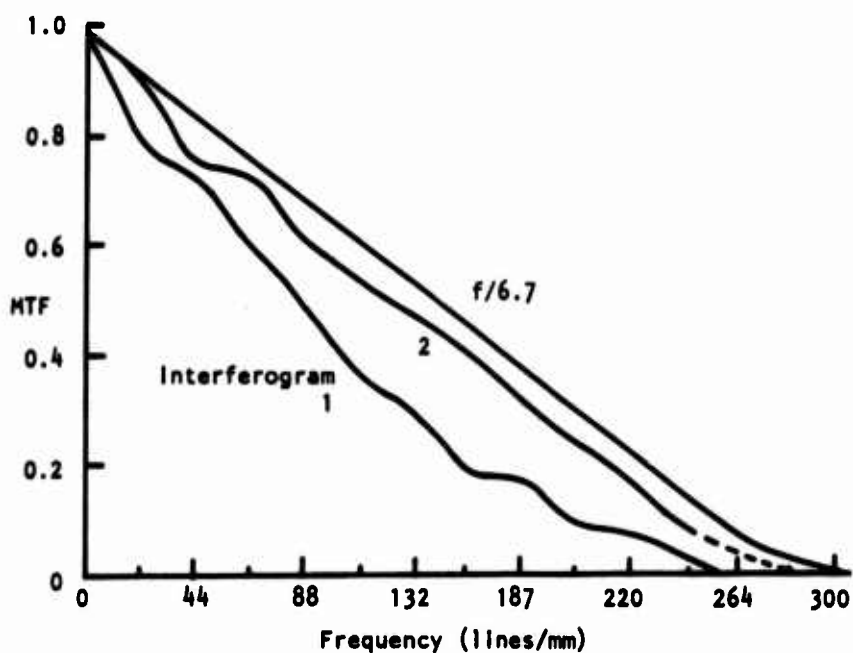
Fig. 12. MTF's Calculated from Two Interferomgrams and a Theoretical
Curve for *f*/6.7 Lens.

consuming process to undertake by hand, and is consequently a process best left to a computer provided an OTF program is available.

It would be helpful if we could assign a number to an interferogram whose value would bear a direct correlation with the image quality obtained, a number that could be obtained quickly and simply without sophisticated computer analysis, and a number that would tell us plainly whether or not the window should be flown. Wavefront variance (or RMS) is a commonly used number to measure quality, but it is not calculated easily. An alternative method is now described.

We know that fringe departure from straightness and equispacing implies image degradation. We now wish to find a measure for this departure. In Fig. 13 we have an enlarged drawing of an interferogram. Through the centralmost fringe, the reference fringe, we have drawn a straight line. The line is drawn such that the cross-hatched area is roughly minimal (eyeball approximation). We then determine the area of the cross hatch by use of a planimeter. The arrows indicate the direction taken by the planimeter, i.e., clockwise around the enclosing curve. We divide this area by the length of the straight line whose ends are defined by its intersection with the edge of the pupil. The resulting number, s, is the average deviation from the straight line. This takes care of one fringe. To obtain an average value, several fringes must be analyzed. The number depends on how the fringes and their spacing vary over the pupil.

The positioning of additional lines cannot be arbitrary but must reflect the wedging present in the window. To find the average spacing,
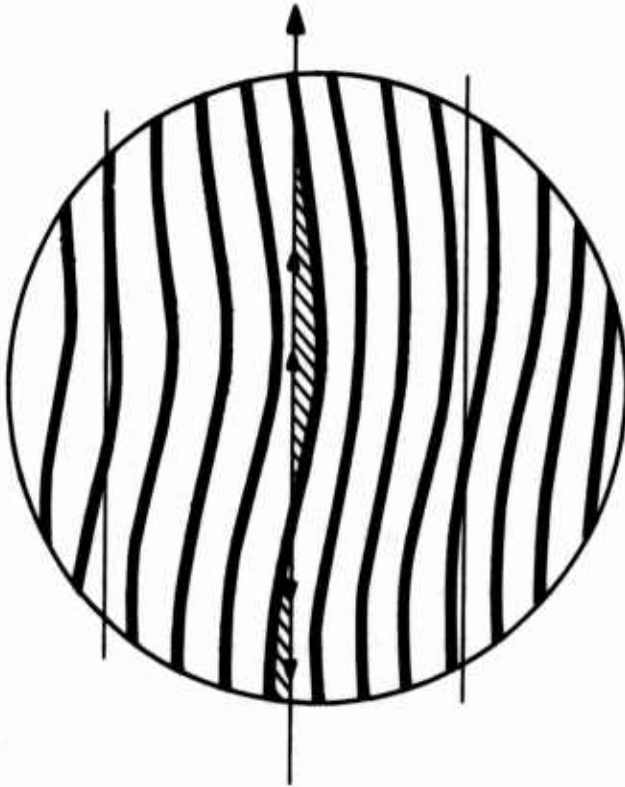
Fig. 13.   Enlarged Drawing of Fig. 9 Showing Planimeter Paths.

S, between lines, we count the total number of spaces between fringes and divide this into the pupil diameter. For Fig. 11 we have 5.92 in. divided by 13.75 spaces, or 0.43 in. per space. The additional lines then must be parallel to the first line with a separation NS, where N is an integer (which in Fig. 11 is 4). The fringe to be associated with this auxiliary line is the fourth fringe over from the reference fringe, which is counted as zero.

Finding the s value for the auxiliary lines for Fig. 11, and then averaging over all the lines analyzed, yields $\bar{s} = \sum_i |s_i|/3 = 0.147$.

We now want to relate this average deviation, $\bar{s}$, to optical path difference. Each fringe in the interferogram is separated from its neighbor by an optical path difference of $\lambda/3$. Therefore S corresponds to $\lambda/3$. We can then set up the ratio

$$\frac{S}{\lambda/3} = \frac{\bar{s}}{\lambda/x} .$$

Solving for x, we have $x = 3S/\bar{s}$. For Fig. 11, $x = 3 \times 0.43/0.147 = 8.78$. Therefore, for Fig. 11, we find the average magnitude of the wavefront deviation to be approximately $\lambda/9$.

Ten windows were analyzed in this way. The results are shown in Table 1. Comparison of the imagery of these figures shows that image quality follows the same ranking. The last four, however, are hard to distinguish from each other. Of the 10 windows analyzed, only d, f, l, and m are considered acceptable for use in flight.

As a general criterion, then, based on the preceding analysis, a window is acceptable if the average magnitude of its wavefront

Table 1. Average Wavefront Deviations
for Selected Windows.

Window	Deviation
b	$\lambda/0.69$
g	$\lambda/0.73$
t	$\lambda/0.89$
e	$\lambda/1.16$
r	$\lambda/1.32$
k	$\lambda/2.01$
d	$\lambda/5.10$
f	$\lambda/6.18$
l	$\lambda/8.78$
m	$\lambda/11.38$

deviation is $\lambda/5$ or less, and unacceptable if the deviation is greater than $\lambda/5$. Note that this criterion is independent of focal length. The only thing that needs to be known about a potential camera system is the maximum aperture that it will subtend on the window. A window may be entirely acceptable for a maximum aperture of 2 in. but totally unacceptable for an aperture of 4 or 5 in.

As already mentioned, wavefront distortions in interferograms are more commonly discussed in terms of variance, V, specifically RMS = $\sqrt{V}$. In polar coordinates, variance across a pupil is defined as

$$V = \frac{\int\limits_{0}^{1}\int\limits_{0}^{2\pi} (\phi-\bar{\phi})^2 \rho d\rho d\theta}{\int\limits_{0}^{1}\int\limits_{0}^{2\pi} \rho d\rho d\theta} = \overline{\phi^2} - (\bar{\phi})^2$$

where ϕ is the *phase* distortion.

The function we have calculated using the planimeter technique is the deviation, defined mathematically as

$$G = \frac{\int\limits_{0}^{1}\int\limits_{0}^{2\pi} |\phi-\bar{\phi}| \rho d\rho d\theta}{\int\limits_{0}^{1}\int\limits_{0}^{2\pi} \rho d\rho d\theta} = \frac{1}{\pi}\left[\int\limits_{0}^{1}\int\limits_{0}^{2\pi} |\phi-\bar{\phi}| \rho d\rho d\theta\right].$$

To obtain an idea of how $\sqrt{V}$ and G compare with each other, cal-
culations for several aberrations were made. The results are presented
in Table 2. It should be noted that the above expression for G is
strictly valid when the fringe spacing in the interferogram is fairly
uniform across the pupil. When this is not true, G is less well defined.
The bull's-eye and hyperbolic fringe patterns fall into the latter
category. However, the planimeter technique was applied to these patterns
successfully. The main question in this regard was what path to follow.
The paths selected by the author for these patterns in his evaluation
are illustrated in Fig. 14. Determination of the pure wedge grid is
the same as previously described, and again the planimeter path is clock-
wise. The determined areas are indicated by cross hatching in Fig. 14.

Table 2. Results of RMS and Deviation Comparison.

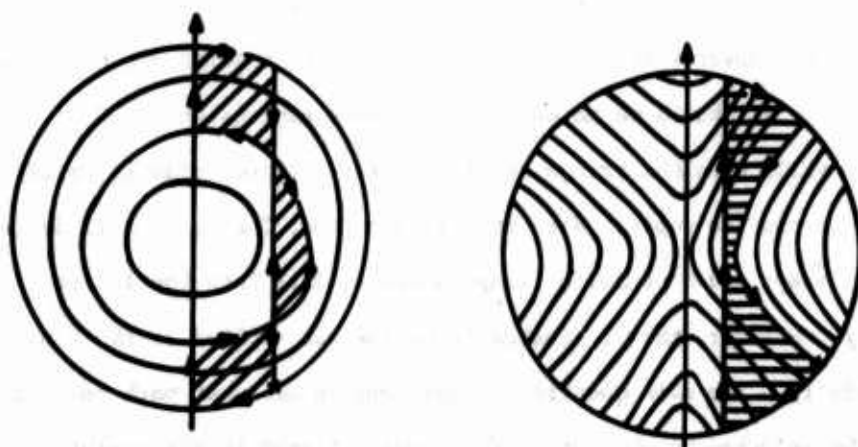| Aberration	ϕ	$\bar{\phi}$	G	$\sqrt{V}$	$G/\sqrt{V}$
Defocus	$A\rho^2$	$\frac{1}{4}A$	$0.250A$	$0.289A$	0.865
Spherical	$B\rho^4$	$\frac{1}{3}B$	$0.257B$	$0.298B$	0.862
Astigmatism	$D\rho^2 \cos^2\theta$	$\frac{1}{4}C$	$0.206C$	$0.250C$	0.824
Astigmatism with defocus	$C\rho^2 \cos2\theta$	0	$0.318C$	$0.408C$	0.779

Fig. 14. Planimeter Paths Selected for Bull's-Eye and Hyperfolic Fringe
Patterns.

Summary

We have seen that a wavefront measuring interferometer provides a convenient tool for acquiring the basic raw data on reconnaissance windows and that the planimeter technique for measuring the deviation of interference fringes allows a quick and simple means of analyzing their performance. The correlation study provides the experimentally based criterion of $\lambda/5$ thickness variation as a cutoff value in window selection.

PRODUCTION OF HIGH EFFICIENCY GRATINGS
FOR A LATERAL SHEAR INTERFEROMETER
(Dave Thomas)

Introduction

The main goal of the experimental work described below was to holographically record gratings of high diffraction efficiency for use in lateral shear interferometers. The frequencies of each pair of gratings making up the lateral shear interferometer were to differ by only about 10%, so as to permit appreciable overlap of the two first diffracted orders. Two particular emulsions, a duPont photopolymer material and dichromated gelatin, were found by other investigators to yield single frequency sinusoidal gratings of high diffraction efficiency and low noise. Preliminary calculations were made on the computer to estimate the optimum diffraction efficiency that could be obtained with the available samples of each emulsion for single frequency gratings. Single frequency gratings were then made in each emulsion at various exposure levels and times, and several double frequency gratings were obtained using the dichromated gelatin emulsion. It was found that composite gratings consisting of two separate gratings made using dichromated gelatin produced an excellent high efficiency lateral shear interferometer. The particular photopolymer material used did not give good gratings.

Apparatus

The apparatus used to construct all gratings is shown on the following page. The two interfering beams were arranged so as to have either one beam normal to the film or both beams make equal angles with the film. The beam angles were adjusted by placing black masks with
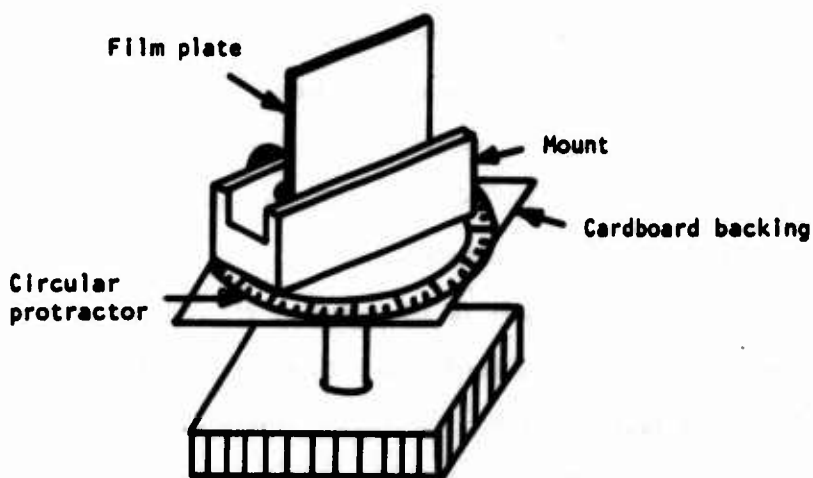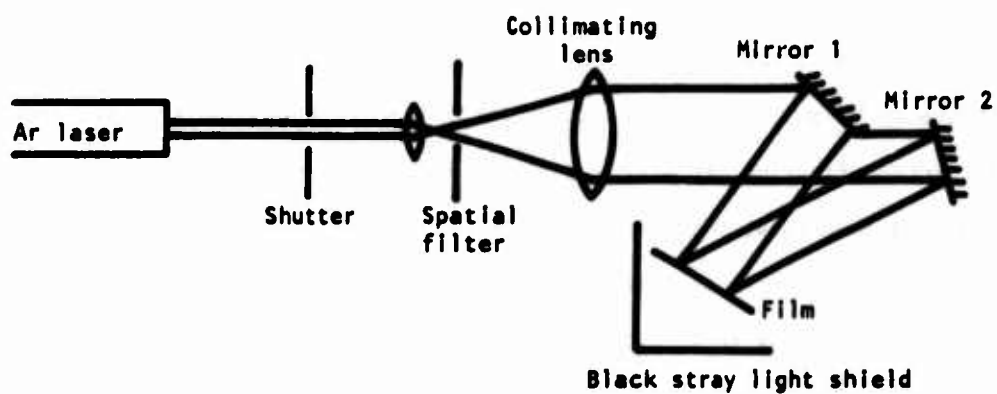
Experimental Setup Used to Produce Holographic Gratings: (above)
Interferometer, (below) Film Holder.

1/4-in.-diameter centered holes over the two mirrors. For the gratings
using a normal reference beam, beam angles were established by placing a
glass plate in the film holder and noting the holder positions relative
to the protractor for which each mask aperture was reflected back on itself
by the plate. When the angular difference between these two positions
was adjusted to the value corresponding to the desired spatial grating
frequency by moving mirror 2, the mount was rotated back to its position
for retroreflection off mirror 1 and locked in place. A similar procedure
was used when equal beam angles to the plate were used to construct the
gratings, but the final plate position for recording was established by
locking the holder in the orientation for which each of the mask apertures
was reflected onto the other. Plate orientations were repeatable to within
about 1/5 degree.

Two frequency gratings were made with a common normal reference
beam. Two mirror positions (corresponding to each of the desired grating
frequencies) were found by the above procedure. The corresponding mirror
positions were marked with templates fixed to the bench surface so that
the mirror could be moved between positions in the dark. The masks were
again removed before the exposures were made.

The photopolymer samples consisted of flexible plastic strips.
These were placed in a cardboard folder that had a window cut in it to
keep the sample flat during exposure. The folder was in turn placed in
the holder. The dichromated gelatin samples were on glass plates iden-
tical to the one used in the above alignment procedure, so they were
mounted directly in the holder.

Procedures

A. *Computer Analysis.* The photopolymer samples tested had thick-
nesses of 1 mil and 3 mil, while the dichromated gelatin emulsions were
15 μm thick. Values for the nominal refractive indices of the two emul-
sions were given by Booth (1975) and Collier et al. (1971) as n_0 (photo-
polymer) = 1.51 and n_0 (gelatin) = 1.52. The computer program utilized
these data and the results of Collier's coupled wave theory development
for single frequency sinusoidal phase gratings in lossless dielectric
emulsions. By assuming that the two interfering collimated beams used to
construct the grating make equal angles with the normal to the emulsion,
Collier arrived at the following formula for diffraction efficiency:

$$\eta = \frac{s_1 n^2 (\xi^2 + \nu^2)^{\frac{1}{2}}}{1 + (\xi^2/\nu^2)}$$

where

$$\xi = \delta \left(\frac{2\pi n_0}{\lambda \alpha}\right) T s_1 n \theta_0$$

$$\nu = \frac{\pi n_1 T}{\lambda \alpha \cos\theta_0}$$

θ_0 = Bragg angle
$\lambda \alpha$ = wavelength in air = 0.5145 μm
T = emulsion thickness
δ = deviation from Bragg angle *in emulsion*
d = grating line spacing
n_1 = amplitude of the index fluctuation about
n_0 in the grating.

The Bragg condition $(2d_a_1 n\theta_0 = \lambda_a/n_0)$ was used with other data to determine the Bragg angle. Values for η were computed using the above formula for various values of δ, n_1, and for spatial frequencies in the 50 to 500-lines/mm range.

B. *Photopolymer Gratings*. The photopolymer material, as described by Booth (1975), had two promising characteristics. Single frequency gratings having diffraction efficiencies of 80 to 90% had been recorded in the material. The gratings could also be developed in place by post-exposure to room light.

The interferometer was set up to produce a 50-line/mm grating by the above-mentioned procedure. The resulting fringes were observed through a microscope before exposing the film to insure stability of the fringes. The interfering beams made equal angles with the normal to the emulsion. Additional experimental parameters for the two samples used were as follows:

```
3 mil emulsion --   beam ratio ∿1:1
                    20 mW at film plane
                    λ = 5145 Å
                    Exposure times: 2 to 9 sec

1 mil emulsion --   beam ratio ∿1:1
                    15 mW at film plane
                    λ = 5145 Å
                    Exposure times: 2 to 7 sec
```

C. *Dichromated Gelatin Gratings*. Lin (1969) explains how sinusoidal gratings are formed in this material. The author obtained single frequency gratings having diffraction efficiencies, η, as high as 90%, but found that gratings having large η values were usually noiser than the lower η gratings. Chang (1971) gave a procedure for preparing the plates from Kodak 649F plates that eliminated the milkiness often encountered with this emulsion.

Our dichromated gelatin plates were prepared using the Chang procedure. The resulting 4-in. by 5-in. plates were cut into fourths and the backs painted with gloss black paint. This paint was removed with a razor blade before the exposed plates were developed.

Single frequency gratings were recorded with a spatial frequency of about 800 lines/mm, while the second grating in the double frequency gratings had a frequency of 900 lines/mm. The beam angles required to produce these frequencies were calculated ($\nu = \sin\theta/\lambda$) to be 24.2° and 27.4°, respectively. The interferometer was adjusted to these values by the aforementioned procedure. Most of the gratings were made with one beam normal to the emulsion.

A 30-sec exposure time with a 0.2-watt laser output was empirically found to give the brightest gratings at 0.5145 μm. Repeated 30-sec exposures with the same laser output were also found to produce the best double frequency gratings.

Several single frequency gratings were also made at $\lambda = 0.4880$ μm. The laser output was again set to 0.2 watt and exposure times of 15 sec, 30 sec, and 45 sec were used.

Results and Discussion

A. *Computer Analysis.* The ν-parameter mentioned in the procedure was found to be fairly insensitive to grating frequency in the range of interest and strongly dependent on the value of n_1 or index modulation. By proper choice of a value for ν, diffraction efficiencies as high as 100% were predicted for no deviation from the Bragg angle ($\delta = 0$). This value fell to as low as 75% for $\delta = 2°$ and $f = 500$ lines/mm. Similarly,

a 100% diffraction efficiency was predicted for the 3-mil photopolymer emulsion for δ = 0 with a falloff to only a few percent at high (500 lines/mm) grating frequencies and δ = 1.5°. The 1-mil photopolymer emulsion differed only in that it suffered less falloff in diffraction efficiency with increasing deviation from the Bragg angle than did the 3-mil emulsion.

As it turned out, the results of this analysis could not be readily compared against the experimental results. One reason for this was that there was no convenient way of measuring the index modulation that existed in the actual gratings. Another reason was that the experimental grating results turned out to be either too poor or inconsistent to permit comparison with theory.

B. *Photopolymer Gratings.* All of the photopolymer gratings obtained were noisy and of low diffraction efficiency. The emulsions themselves were observed to have a bubbly surface texture. The manufacturer was contacted, and it was learned that the available samples had far exceeded the manufacturer's suggested shelf life. This was taken to be the reason for the poor experimental results. It has not been possible to obtain new samples of the photopolymer.

C. *Dichromated Gelatin Gratings.* The most encouraging results were obtained with this emulsion, but some unexpected problems were encountered.
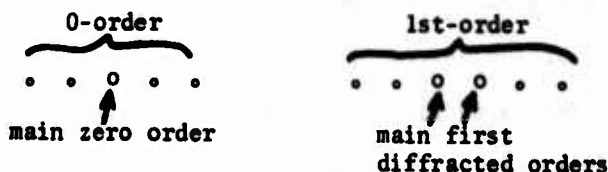
The plates were all prepared by the Chang (1971) procedure and were generally clear and non-milky. An occasional batch of plates did, however, turn out to be milky. This effect was most severe when the

Kodak 649F plates had been left unrefrigerated for several days before starting the processing procedure. Since the mechanical properties of the gelatin determine how the emulsion will behave when it goes through the development process, it is possible that this prolonged exposure to room temperatures could have caused the resulting milkiness. These milky plates also tended to develop with finely spaced vertical cracks over the face of the grating that scattered a great deal of light.

The single frequency gratings generally fell into two categories: they either had low diffraction efficiencies (5 to 15%) and low noise, or high diffraction efficiencies (75 to 90%) and high noise. A few gratings having diffraction efficiencies in the 40 to 60% range with both low and high amounts of noise were also obtained. The fact that the brightest gratings were also the noisiest is consistent with Lin's findings. All gratings were made under the same exposure conditions (30-sec exposure time, 0.2-watt laser output). In addition to this variation in diffraction efficiency from exposure to exposure, there was variation over the surface of many of the gratings themselves of up to 40% or so. In these gratings, random areas of low diffraction efficiency were interspersed with the high η regions. The cause for both the nonuniformity of the gratings and their variation from exposure to exposure probably had something to do with the way they were processed or the nature of the original 649F plates. These variations were noted regardless of the exposure time or laser output level used. The gratings made with 0.4880-μm light achieved a maximum diffraction efficiency of only 15%. The exposure time required to produce the brightest gratings at this wavelength was around 15 sec as opposed to the

30-sec exposure time required to produce bright gratings at $\lambda = 0.5145$ μm.
These gratings all had low noise, and they demonstrated the same varia-
tions in diffraction efficiency that were observed at the longer wavelength.

The two-frequency gratings were made at $\lambda = 0.5145$ μm. Shortly
after development, these gratings were observed to transmit two equally
bright first-order beams (one corresponding to each frequency) when illumi-
nated by the common normal reference beam. The diffraction efficiency of
each individual grating was low at this point, but when a beam was focused
onto the grating by an aberrated lens, a dim but good contrast lateral
shear interferogram of the aberrated wavefront was observed in the region
of overlap of the two first orders. When the gratings were allowed to dry
for several hours and observed again, it was found that the two side orders
had become brighter. Unfortunately, additional orders were also present
that were not attributable to either of the two component gratings. The
diffraction pattern observed when the double frequency gratings were illumi-
nated with a laser beam was somewhat as shown below:

<div style="text-align:center">

0-order   1st-order

• • O • •   • • O O • •

main zero order   main first
                             diffracted orders

</div>

The angular separation between adjacent spots within each order was mea-
sured on a goniometer to be approximately the same value for all pairs.

The additional orders are believed to be due to coupling between
the two sets of grating planes. This coupling becomes more pronounced and
the additional orders brighter as the diffraction efficiencies of the

component gratings are increased. Aberrated wavefronts focused onto these "dryer" double frequency gratings resulted in several closely spaced lateral shear interferograms. The additional interferograms destroyed the contrast of the one of interest.

This effect was not observed when two different single frequency gratings were pressed against each other to form a composite grating. A composite grating made using two single frequency gratings each having a diffraction efficiency of nearly 60% gave very bright, high contrast lateral shear interferograms when aberrated wavefronts were focused on it. Both the 0,0;1,-1 and 0,1;1,0 diffraction orders gave excellent lateral shear interferograms. Since each pair of diffraction orders gave an efficiency of approximately 30%, if the two pairs of diffraction orders are used in a heterodyne lateral shear interferometer, 60% of the incident energy could be utilized, which is several times the efficiency of previous grating lateral shear interferometers.

References

Booth, B. L., "Photopolymer Material for Holography," Appl. Opt. 14, 593 (1975).

Chang, M., "Dichromated Gelatin of Improved Optical Quality," Appl. Opt. 10, 2550 (1971).

Collier, R. J., Burckhardt, C. B., and Lin, L. H., Optical Holography (Academic Press, N.Y., 1971).

Lin, L. H., "Hologram Formation in Hardened Dichromated Gelatin Films," Appl. Opt., 8, 963 (1969).

SAMSO TECHNICAL REPORT DISTRIBUTION LIST

One copy to each addressee unless otherwise indicated

HQ USAF (AFRDSA)
Washington, D.C. 20330

HQ USAF (AFRDSD)
Washington, D.C. 20330

Secretary of the Air Force (SAFRD)
Washington, D.C. 20330

HQ AFSC (DLSS)
Andrews AFB
Washington, D.C. 20331

HQ USAF (AFRDR)
Washington, D.C. 20330

Capt. Edward Dietz   (9 copies)
SAMSO/DYS
P.O. Box 92960
Worldway Postal Center
Los Angeles, California 90009

Defense Documentation Center (DDC)   (12 copies)
Cameron Station
Alexandria, Virginia 22314

Air University Library
Maxwell AFB, Alabama 36112

Air Force Avionics Laboratory
Wright-Patterson AFB, Ohio 45433   (2copies, 1 to AVRO)

Air Force Cambridge Research Laboratory (CRO)
L. G. Hanscom Field
Bedford, Massachusetts 01730

Aeronautical Systems Division (ASRS)
Wright-Patterson AFB, Ohio 45433

Air Force Office of Scientific Research (SRPP)
1400 Wilson Blvd.
Arlington, Virginia 22209

Air Force Weapons Laboratory (LRO)
Kirtland AFB, New Mexico 87117

David Smith   (3 copies)
Itek Corporation
Lexington, Massachusetts 02173

Rod Scott   (3 copies)
Perkin Elmer Corporation
50 Danbury Road
Norwalk, Connecticut 06851

Sarah Hise
SAMSO/DYK
P.O. Box 92960
Worldway Postal Center
Los Angeles, California 90009